NUCL SCI TECH (2016) 27:124
DOI 10.1007/s41365-016-0107-5

Theoretical investigation of uranium(IV) coordinated with *N*, *N′*- bis(3-allyl salicylidene)-o-phenylenediamine

Wen-Bo Lan[1] · Sha Gao[1] · Ying-Wu Lin[1] · Guo-Wen Peng[1] · Chang-Ming Nie[1]

Received: 14 December 2015 / Revised: 15 March 2016 / Accepted: 25 March 2016 / Published online: 3 September 2016

Abstract We used density functional theory calculations at the B3LYP/6-311G** level for a theoretical study on the complex formed when uranium(IV) coordinates with *N*, *N′*- bis(3-allyl salicylidene)-o-phenylenediamine (BASPDA), i.e., U(BASPDA)$_2$. The results indicated that the coordination complex of U(BASPDA)$_2$ could form two different structures with a ratio of 1:2. One was a parallel dislocation structure (PDS-U), in which the two BASPDAs' middle benzene rings adopted a parallel dislocation with an angle of 56.64°, and the other was a staggered finger "+" structure (SFS-U), in which the two BASPDAs employed the staggered finger "+" shape. The binding energies, charge distribution, spectral properties, thermodynamic properties, molecular orbitals and Wiberg bond indices for both PDS-U and SFS-U were calculated and compared with each other.

Keywords Density functional theory · *N*, *N′*- bis(3-allyl salicylidene)-o-phenylenediamine · Uranium

1 Introduction

Uranium is a toxic radionuclide with a special configuration similar to thorium in which the 5f orbital energy level is very close to the 6d [1]. The 5f orbitals could also participate in bonding, and thus, uranium and thorium can form host multiple ligands in similar configurations [2–4]. During the development of computational chemistry [5, 6], density functional theory (DFT) [7–10] was continuously introduced into the polymerization of molecular imprinting [11–15]. Computer simulations can partially replace conventional experiments and greatly reduce the number of synthesis conditions and the cost of reagents and labor. Some important uranium complexes have been reported using density functional theory (DFT) calculations with the B3LYP method of 6-311G** basis set [16]. These have offered valuable synthetic guides.

N, *N′*-bis(3-allyl salicylidene)-o-phenylenediamine (BASPDA) is an important Schiff base with four coordination atoms. A thorium complex of BASPDA, Th(BASPDA)$_2$, was synthesized in the laboratory [17]. While uranium has a similar coordination property as thorium, there has been no study on U(BASPDA)$_2$. In this paper, we performed a theoretical study on U(BASPDA)$_2$ using DFT calculations with the B3LYP method on a 6-311G** basis set. Some important structural information and properties of U(BASPDA)$_2$ were obtained including the molecular configuration parameters, spectral properties, thermodynamic properties, atomic charge, molecular orbitals and binding energy.

2 Methods

Geometry optimization used Gaussian 09 software [18]. Density functional theory (DFT) [19] calculations for the U(BASPDA)$_2$ complexes are shown in Figs. 1 and 2 via the B3LYP [20] gradient-corrected hybrid function to solve the Kohn–Sham equations with a 10^5 convergence criterion for the density change. Relativistic effects were considered through the use of RECP basis sets [21, 22] on the U atom.

✉ Chang-Ming Nie
niecm196132@163.cm

[1] School of Chemistry and Chemical Engineering, University of South China, Hengyang 421001, China

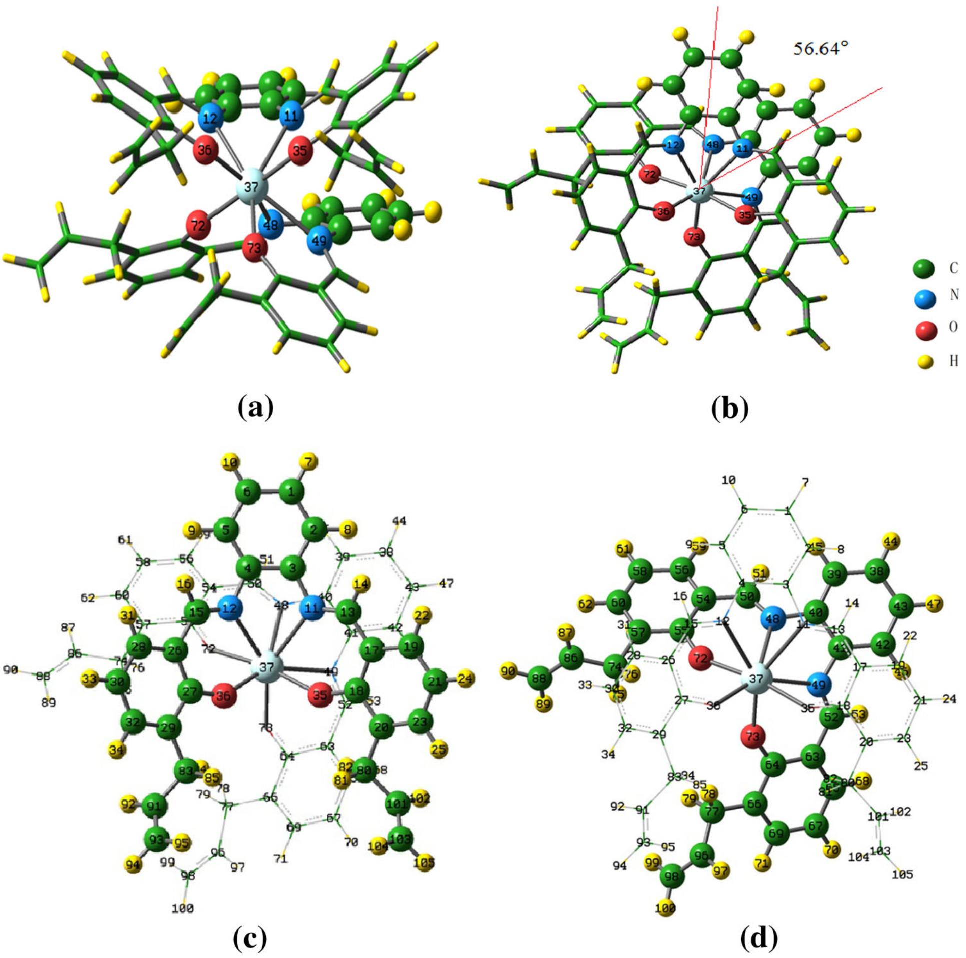

Fig. 1 The optimized configuration of the PDS-U. **a** Front view, **b** top view, **c** bottom view and **d** top view

For the other atoms (C, H, O, N), the 6-311G** basis sets [23] were adopted. The final geometries were confirmed as minima of the potential energy surface (PES) by calculating the Hessians. The harmonic vibrational frequencies and intensities were calculated at the same level of theory using the second derivatives of the energy as a function of atomic coordinates. The calculated intensities generated the theoretical spectra. The main structural parameters and infrared characterization from the theoretical simulation for PDS-U of $U(BASPDA)_2$ complex were compared and analyzed with the corresponding SFS-U.

3 Results and discussion

3.1 The PDS-U and the SFS-U structures

The molecular simulation was performed using DFT calculations [19] at the B3LYP [20]/6-311G** level for $U(BASPDA)_2$. The results showed that uranium (IV) could be coordinated by two BASPDA molecules. These formed a complex of $U(BASPDA)_2$ with two different structures and a ratio of 1:2. The optimized configurations are shown in Figs. 1 (PDS-U) and 2 (SFS-U), respectively. Figure 1a, b show the two different perspectives, i.e., the front view and the top view, respectively. The two BASPDA molecules lay upward and downward at the uranium in similar "∨" and "∧" shapes, respectively. The two BASPDAs' middle benzene rings (the benzene rings of o-phenylenediamine) adopted a parallel dislocation structure (PDS) with an angle of 56.64°, and uranium(IV) occupied the central position of the molecular structure. The numbers of atoms are listed in Fig. 1c, d, c and d as the top view and bottom view of the PDS-U, respectively. The other $U(BASPDA)_2$ structures are shown in Fig. 2. Uranium(IV) coordinated with four nitrogen atoms and four oxygen atoms of the two BASPDA molecules give a staggered finger "+" structure (SFS). In the SFS, the benzene rings of o-phenylenediamine of BASPDAs were perpendicular to each other, and the transverse BASPDA molecule was similar to "∨" shape. The uranium ion is located at the center of the "+" shape. The numbers of atoms are listed in Fig. 2c, d. This figure shows the top view (b) and front view (a), (c) shows the number of transverse BASPDA ligands, and (d) is the number of the vertical BASPDA for the SFS-U.

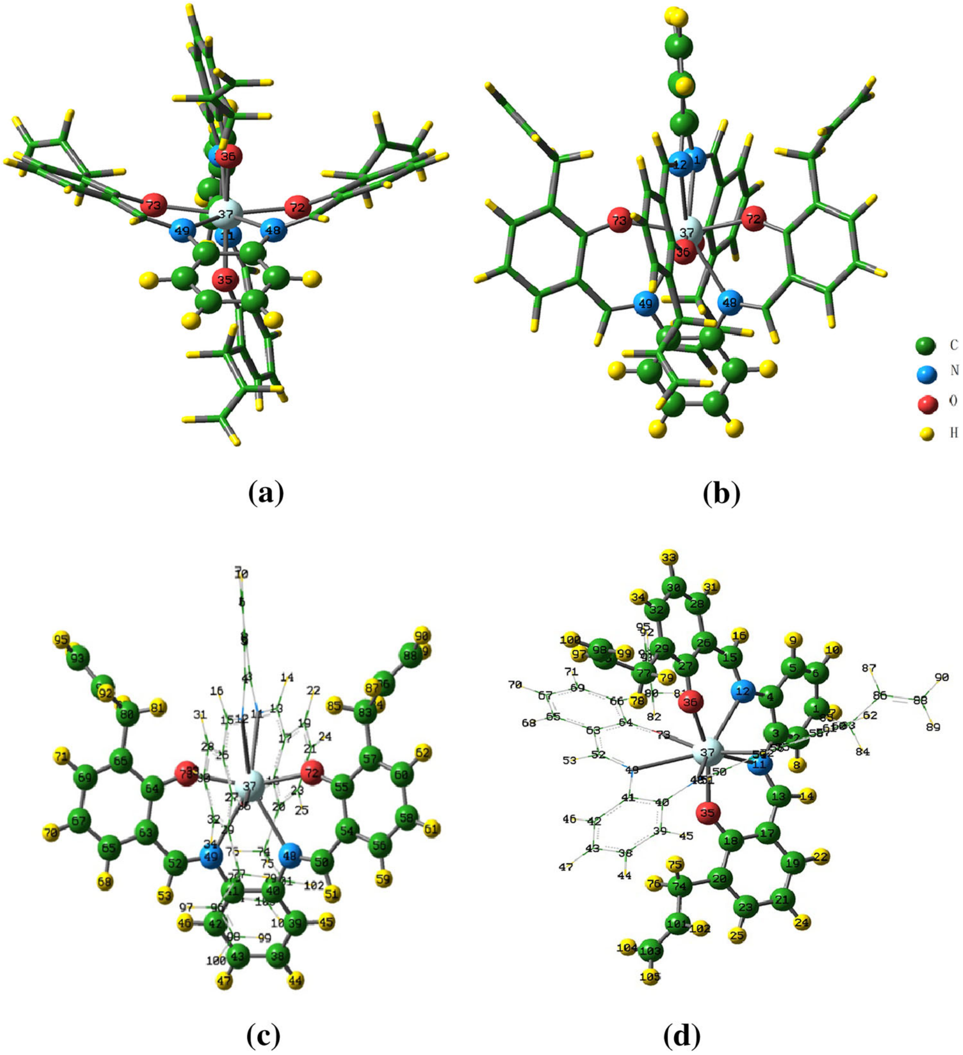

Fig. 2 The optimized configuration of the SFS-U. **a** Front view, **b** top view, **c** top view and **d** right side view

Table 1 The calculated bond lengths of the PDS-U and the SFS-U, and the experimental data for PDS-Th [17]

Bond length(Å)	PDS-U	PDS-Th	SFS-U	Bond length	PDS-U	PDS-Th	SFS-U
U–O(35)	2.2303	2.286	2.2278	U–N(11)	2.6881	2.651	2.6089
U–O(36)	2.2243	2.265	2.2142	U–N(12)	2.6604	2.665	2.6765
U–O(72)	2.2303	2.266	2.2279	U–N(48)	2.6884	2.671	2.6213
U–O(73)	2.2243	2.259	2.2234	U–N(49)	2.6606	2.665	2.6302

As shown in Fig. 2, different balls stand for N, O, C and H atoms, including the center U atom. The main structural parameters from the molecular simulation are shown in Tables 1 and 2.

The calculated bond lengths and bond angles for the PDS-U and the SFS-U are listed in Tables 1 and 2. It was clear that the PDS-U was totally different from the SFS-U, in which the two BASPDA ligands combined with a U atom such that the middle benzene ring had a parallel dislocation angle of 56.64°. Although the main bond lengths of the PDS-U were close to the SFS-U, the main bond angles were totally different from each other. This implied that there were two different structures for U(BASPDA)$_2$.

There were no experimental data available for U(BASPDA)$_2$. Thus, we compared the calculated results with that of Th(BASPDA)$_2$ as recently synthesized by He et al. [17]. Note that only one structure of PDS-Th was obtained in their experiment (Tables 1 and 2). The comparison showed that the calculated parameters for PDS-U are very similar to that of PDS-Th, confirming the accuracy of our calculations.

Table 2 The calculated bond angles of the PDS-U and the SFS-U, and the experimental data for PDS-Th

Bond angle(°)	PDS-U	PDS-Th	SFS-U	Bond angle	PDS-U	PDS-Th	SFS-U
O(35)–U–O(36)	87.4	88.02	155.39	O(72)–U–N(12)	74.48	74.27	80.67
O(35)–U–O(72)	171.2	172.09	95.89	O(73)–U–N(12)	151.68	154.07	76.53
O(35)–U–O(73)	86.31	86.03	96.69	O(35)–U–N(11)	67.77	67.94	70.69
O(36)–U–O(72)	86.32	85.26	87.89	O(36)–U–N(11)	106.92	110.73	133.77
O(36)–U–O(73)	88.86	90.62	88.78	O(72)–U—N(11)	120.08	118.48	76.27
O(72)–U–O(73)	87.4	89.87	156.71	O(73)–U–N(11)	148.4	144.87	86.53
N(11)–U–N(12)	58.75	60.30	64.16	O(35)–U–N(48)	120.07	120.02	80.88
N(11)–U–N(48)	73.71	70.60	134.84	O(36)–U–N(48)	148.4	147.62	77.74
N(11)–U–N(49)	86.44	81.55	139.51	O(72)–U–N(48)	67.77	67.64	69.37
N(12)–U–N(48)	86.45	87.03	136.41	O(73)–U–N(48)	107.92	106.07	132.11
N(12)–U–N(49)	137.44	136.67	134.3	O(35)–U–N(49)	74.47	72.92	80.04
N(48)–U–N(49)	58.75	59.66	63.01	O(36)–U–N(49)	151.69	151.90	77.74
O(35)–U–N(12)	108.87	107.02	134.59	O(72)–U–N(49)	108.87	111.74	132.28
O(36)–U–N(12)	68.77	68.11	70.02	O(73)–U–N(49)	68.78	68.10	69.43

3.2 Atomic charge distribution

The atomic charges obtained from the simulation for the PDS-U and the SFS-U are listed in Table 3. The numbers of atoms are shown in Figs. 1c, d and 2c, d. The positive electric charge values of U in the PDS-U and the SFS-U are +2.4009 and +2.3934, respectively. This indicates that the donor atoms in the PDS-U and the SFS-U could coordinate with the uranium ion with different binding modes.

3.3 Infrared spectroscopy

The infrared spectra of the PDS-U and the SFS-U obtained by molecular simulations at the same level are shown in Fig. 3. There was no imaginary frequency for the calculated IR vibrations of all geometry structures. This indicated that these two structures are quite stable. The C=N stretching vibration absorption peak of the PDS-U appeared at 1638.75 cm^{-1}, and the benzene ring stretching vibration absorption peak was at 1574.06 cm^{-1}. These observations are similar to that for the PDS-Th complex in the experiment, i.e., 1612 and 1574 cm^{-1}, respectively [17]. For the SFS-U complex, the C=N stretching vibration absorption peak appeared at 1640.98 cm^{-1}, and the benzene ring stretching vibration absorption peak was at 1574.30 cm^{-1}. These were very close to the corresponding peak for the PDS-U complex. However, the absorption intensities were significantly different, and the benzene ring stretching vibration absorption of the PDS-U was stronger than that of the SFS-U.

3.4 Binding energy

The binding energies of the PDS-U and SFS-U complexes were calculated. The binding energy was calculated via formula (1). The term $\Delta_{AB}W(R)$ represents the binding energy, and $\overline{W}_{AB}(R)$ stands for the total energy of the interacting system. Terms $\overline{W}_A$ and $\overline{W}_B$ stand for the energies of the two separate molecules A and B, respectively.

$$\Delta_{AB}W(R) = \overline{W}_{AB}(R) - \overline{W}_A - \overline{W}_B \tag{1}$$

The binding energies of the PDS-U and SFS-U were −4695.95 and −4760.61 kJ/mol. The binding energy of the SFS-U was −64.66 kJ/mol smaller than that of the PDS-U. This means that the *N*, *N*′- bis(3-allyl salicylidene)-o-phenylenediamine coordinated more strongly with uranium (IV) in the SFS-U complex than in the PDS-U complex.

3.5 The thermal properties of complexes

To further investigate the stability of the two complexes, we calculated the changes of Gibbs free energy (ΔG) and enthalpy (ΔH) for the complexation reactions (U^{4+} + 2BASPDA → $U(BASPDA)_2 + 2H^+$) under the same model. Table 4 shows the calculated thermal properties for the PDS-U and the SFS-U of $U(BASPDA)_2$ at 298.15 K and 1 atm. The results showed that SFS-U has a ΔG value that is ~64 kJ/mol lower than that of PDS-U; the ΔH value is ~63 kJ/mol lower than that of PDS-U. These results indicated that SFS-U is more stable than PDS-U and the BASPDA ligand coordinates more tightly with U(IV) in the SFS-U complex versus PDS-U complex.

3.6 Molecular orbitals and energies

Figure 4 presents the Kohn–Sham representations of HOMO (the highest occupied molecular orbital) and LUMO (the lowest unoccupied molecular orbital) for the PDS-U and the SFS-U of $U(BASPDA)_2$. The red and green

Table 3 The atomic charge comparison of the PDS-U with the SFS-U

N	Charge		*N*	Charge		*N*	Charge	
	PDS-U	SFS-U		PDS-U	SFS-U		PDS-U	SFS-U
C-1	−0.1004	−0.0843	O-36	−0.6110	−0.6344	H-71	0.0937	0.0935
C-2	−0.0829	−0.1143	U-37	2.4009	2.3934	O-72	−0.6248	−0.6291
C-3	0.1385	0.1906	C-38	−0.1004	−0.0751	O-73	−0.6110	−0.6280
C-4	0.1428	0.1801	C-39	−0.0829	−0.1161	C-74	−0.1200	−0.1215
C-5	−0.0884	−0.1035	C-40	0.1384	0.1660	H-75	0.1291	0.1820
C-6	−0.0896	−0.0843	C-41	0.1428	0.1691	H-76	0.1660	0.1236
H-7	0.0943	0.0959	C-42	−0.0884	−0.0953	C-77	−0.1426	−0.1253
H-8	0.1070	0.1099	C-43	−0.0896	−0.0841	H-78	0.1722	0.1507
H-9	0.1028	0.1018	H-44	0.0943	0.0961	H-79	0.1272	0.1260
H-10	0.0964	0.0953	H-45	0.1070	0.1071	C-80	−0.1200	−0.1280
N-11	−0.5111	−0.5733	H-46	0.1028	0.1072	H-81	0.1291	0.1645
N-12	−0.5387	−0.5567	H-47	0.0964	0.0961	H-82	0.1661	0.1259
C-13	0.1824	0.1822	N-48	−0.5110	−0.5566	C-83	−0.1425	−0.1266
H-14	0.0930	0.0977	N-49	−0.5386	−0.5568	H-84	0.1722	0.1237
C-15	0.1892	0.1767	C-50	0.1824	0.1857	H-85	0.1272	0.1631
H-16	0.0956	0.0908	H-51	0.0930	0.0945	C-86	−0.1628	−0.1657
C-17	−0.1776	−0.1748	C-52	0.1893	0.1770	H-87	0.0961	0.0998
C-18	0.2801	0.2873	H-53	0.0956	0.0947	C-88	−0.1928	−0.1931
C-19	−0.0380	−0.0445	C-54	−0.1775	−0.1778	H-89	0.0979	0.0972
C-20	−0.1937	−0.1851	C-55	0.2801	0.2934	H-90	0.1021	0.1024
C-21	−0.1119	−0.1093	C-56	−0.0380	−0.0435	C-91	−0.1625	−0.1665
H-22	0.0809	0.0822	C-57	−0.1937	−0.1856	H-92	0.1010	0.0981
C-23	−0.0186	−0.0166	C-58	−0.1119	−0.1095	C-93	−0.1927	−0.1923
H-24	0.0870	0.0868	H-59	0.0809	0.0825	H-94	0.1031	0.0981
H-25	0.0930	0.0922	C-60	−0.0186	−0.0147	H-95	0.0969	0.1022
C-26	−0.1795	−0.1809	H-61	0.0870	0.0869	C-96	−0.1625	−0.1652
C-27	0.2775	0.2972	H-62	0.0930	0.0932	H-97	0.1010	0.1001
C-28	−0.0435	−0.0411	C-63	−0.1795	−0.1835	C-98	−0.1927	−0.1932
C-29	−0.1764	−0.1875	C-64	0.2775	0.2929	H-99	0.0969	0.0974
C-30	−0.1078	−0.1097	C-65	−0.0435	−0.0418	H-100	0.1031	0.1032
H-31	0.0811	0.0813	C-66	−0.1763	−0.1864	C-101	−0.1628	−0.1672
C-32	−0.0091	−0.0118	C-67	−0.1078	−0.1092	H-102	0.0961	0.0976
H-33	0.0871	0.0870	H-68	0.0811	0.0829	C-103	−0.1928	−0.1952
H-34	0.0937	0.0931	C-69	−0.0091	−0.0117	H-104	0.0979	0.0971
O-35	−0.6248	−0.6242	H-70	0.0871	0.0861	H-105	0.1021	0.1015

portions represent the positive and negative phase of the molecular orbitals, respectively.

The highest occupied molecular orbital energy (E_{HOMO}) of the PDS-U is shown on the left in Fig. 4 and was −3.7889 eV. The lowest unoccupied molecular orbital energy (E_{LUMO}) of the PDS-U is shown on the right and was −2.2903 eV. The energy gap between LUMO and HOMO was 1.4985 eV, namely $\Delta E = 1.4985$ eV. This indicated that to get the excited PDS-U, an energy of 1.4985 eV would be absorbed by the ground-state molecule. For SFS-U, E_{HOMO} was −4.1296 eV, and the E_{LUMO} was −2.1075 eV; the energy gap (ΔE) was 2.0221 eV—this indicated that 2.0221 eV would be absorbed when the ground-state SFS-U was excited. Thus, the ground state of SFS-U is harder to excite than the ground state of PDS-U. The SFS-U complex is thus more stable than the PDS-U complex (Table 5).

The HOMO energies were negative in the two U(BASPDA)$_2$ complexes. This implied that the extent of electron delocalization increased after the complex formation. The energies of the occupied orbitals decreased, and stability was enhanced in the system.

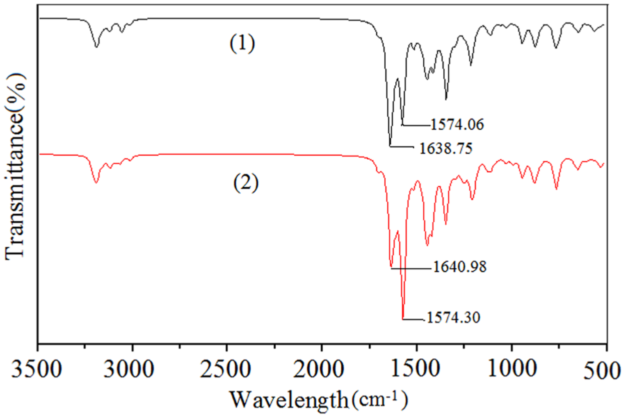

Fig. 3 Infrared spectra of the PDS-U and the SFS-U. Curve (*1*) was PDS-U and curve (*2*) is SFS-U

Table 4 The change in thermodynamic data for the PDS-U and the SFS-U (KJ/mol) at 298.15 K and 1 atm

Structure	PDS-U	SFS-U
ΔG	−4819.58	−4883.80
ΔH	−4869.49	−4932.60

Table 5 The energy of E_{HOMO}, E_{LUMO} and $\Delta E_{\mathrm{L-H}}$ for the PDS-U and the SFS-U (eV)

Structure	E_{HOMO}	E_{LUMO}	$\Delta E_{\mathrm{H-L}}$
PDS-U	−3.7889	−2.2904	1.4985
SFS-U	−4.1296	−2.1075	2.0221

Table 6 The Wiberg bond indices (WBIs) of U–O and U–N for the PDS-U and the SFS-U

WBIs	PDS-U	SFS-U	WBIs	PDS-U	SFS-U
U–O(35)	0.7310	0.7415	U–N(11)	0.3508	0.3948
U–O(36)	0.7179	0.7581	U–N(12)	0.3620	0.3700
U–O(72)	0.7359	0.7478	U–N(48)	0.3659	0.3819
U–O(73)	0.7238	0.7534	U–N(49)	0.3678	0.3813

3.7 Wiberg bond order indices

Generally, larger bond orders have larger bond energy and more stability [24]. Table 6 shows that the U–O WBIs

Fig. 4 Molecular orbitals and energies of the PDS-U and the SFS-U. **a** HOMO of the PDS-U (−3.7889 eV), **b** LUMO of the PDS-U(−2.2904 eV), **c** HOMO of the SFS-U(−4.1296 eV) and **d** LUMO of the SFS-U(−2.1075 eV)

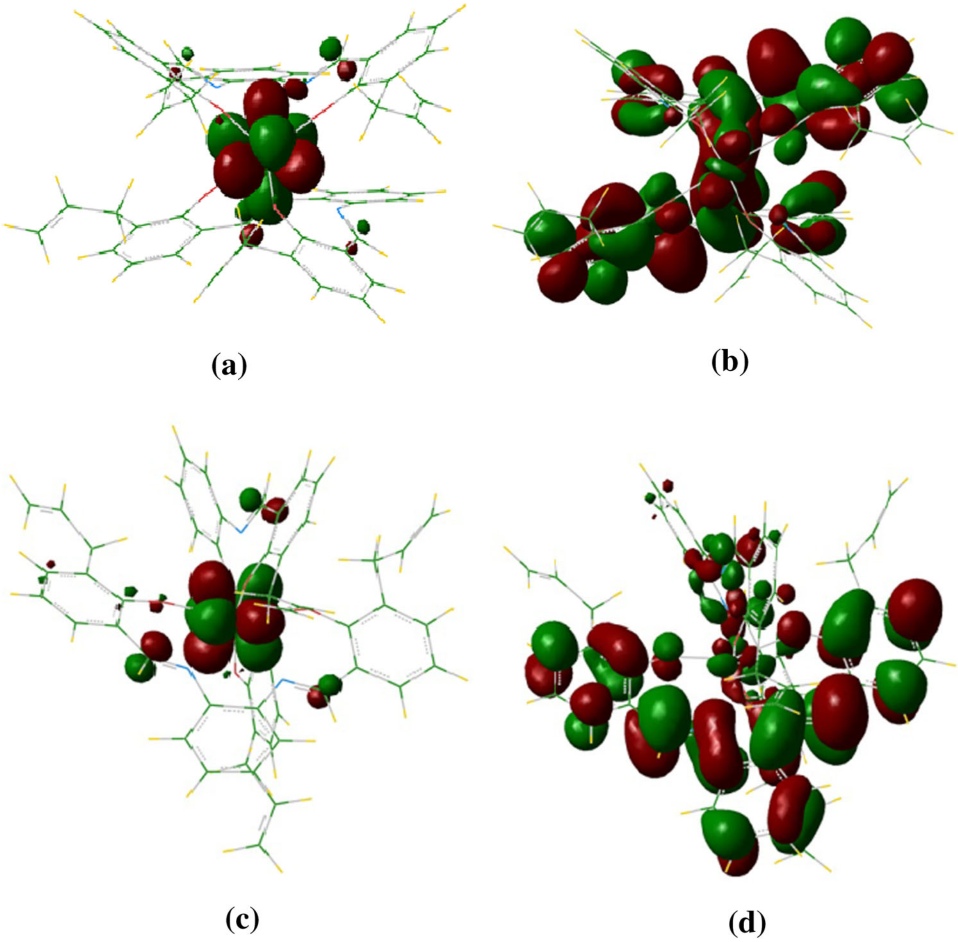

ranged from 0.7179 to 0.7581 for the complexes on the same basis of NBO (natural bond orbital). The U–N WBIs changed from 0.3508 to 0.3948. The U–O Wiberg bond indices (WBIs) of the complexes were higher than the U–N Wiberg bond indices. This showed that the U–O bonds have more covalent characters than the U–N bonds. For the PDS-U complex, the WBIs of both the U–O bonds and U–N bonds were slightly less than those of the SFS-U complex. This indicated that the strengths of the U–O and U–N bonds in SFS-U complex were slightly stronger than that in the PDS-U complex.

4 Conclusion

A complex of uranium(IV)–Schiff base, U(BASPDA)$_2$, was theoretically studied using DFT calculations at the B3LYP/6-311G** level including the molecular geometry, atomic charge, spectral properties, binding energy, thermodynamic properties and molecular orbitals. The complex U(BASPDA)$_2$ could form two different molecular structures with a ratio of 1:2. One was the PDS-U structure in which the two middle benzene rings of BASPDA (the benzene rings of o-phenylene-diamine) adopted a parallel dislocation with an angle of 56.64°. The other was the SFS-U structure in which the two BASPDA molecules constructed a similar staggered finger “+” shape. The results further indicated that SFS-U is more stable than PDS-U. The BASPDA ligand coordinated more tightly with the U(IV) in the SFS-U complex versus that in the PDS-U complex. This study provides theoretical guidelines for the synthesis of other uranium complexes in experimental applications.

Acknowledgments This work is supported by National Natural Science Foundation of China (No: 11275090, 51574152), Hunan Provincial Natural Science Foundation for Distinguished Young Scholars (2015JJ1012) and Scientific Research Fund of Hunan Provincial Education Department, China (12A116).

References

1. C.Y. Zhou, C.M. Nie, S. Li et al., Chemical behavior of topology and its application to QSPR of lanthanide and actinide[J]. Chin. J. Inorg. Chem. **23**, 25–33 (2007)
2. A.L. Ward, W.W. Lukens, C.C. Lu et al., Photochemical route to actinide-transition metal bonds: synthesis, characterization and reactivity of a series of thorium and uranium heterobimetallic complexes[J]. J. Am. Chem. Soc. **136**, 3647–3654 (2014). doi:10.1021/ja413192m
3. M.J. Monreal, R.J. Wright, D.E. Morris et al., Thorium(IV) and uranium(IV) halide complexes supported by bulky β-diketiminate ligands[J]. Organometallics **32**, 1423–1434 (2013). doi:10.1021/ja413192m
4. A.C. Behrle, C.L. Barnes, N. Kaltsoyannis et al., Systematic investigation of thorium(IV)- and uranium(IV)- ligand bonding in dithiophosphonate, thioselenophosphinate, and diselenophosphonate complexes[J]. Inorg. Chem. **52**, 10623–10631 (2013). doi:10.1021/ic401642a
5. A.D. Becke, Density-functional thermochemistry. III. The role of exact exchange[J]. J. Chem. Phys. **98**, 5648–5652 (1993). doi:10.1021/ic401642a
6. I.Y. Zhang, J. Wu, X. Xu, Extending the reliability and applicability of B3LYP[J]. Chem. Commun. **46**, 3057–3070 (2010). doi:10.1039/c000677g
7. E. Regulska, M. Kalinowska, S. Wojtulewski et al., Theoretical (in B3LYP/6-3111 ++G** level), spectroscopic (FT-IR, FT-Raman) and thermogravimetric studies of gentisic acid and sodium, copper(II) and cadmium(II) gentisates[J]. Spectrochim. Acta Part A **132**, 713–725 (2014). doi:10.1016/j.saa.2014.04.191
8. E. Talebian, M. Talebian, A comparative DFT study on the differences between normal modes of polyethylene and polyethylene glycol via B3LYP Hamiltonian and the Hartree-Fock method in multiple bases[J]. Optik-Int. J. Light Electron Opt. **125**, 228–231 (2014). doi:10.1016/j.ijleo.2013.06.095
9. G.R. Feng, T.Y. Qi, W.J. Shi et al., A B3LYP and MP2(full) theoretical investigation on the cooperativity effect between hydrogen-bonding and cation-molecule interactions and thermodynamic property in the 1: 2 (Na(+): N-(Hydroxymethyl)acetamide) ternary complex[J]. J. Mol. Model. **20**, 1–12 (2014). doi:10.1016/j.ijleo.2013.06.095
10. L. Wu, B. Sun, Y. Li et al., Study properties of molecular imprinting polymer using a computational approach[J]. Analyst **128**, 944–949 (2003). doi:10.1039/b212731h
11. L. Wu, Y. Li, Study on the recognition of templates and their analogues on molecularly imprinted polymer using computational and conformational analysis approaches[J]. J. Mol. Recognit. JMR **17**, 567–574 (2004). doi:10.1002/jmr.688
12. E.R. Mojica, Screening of different computational models for the preparation of sol-gel imprinted materials[J]. J. Mol. Model. **19**, 3911–3923 (2013). doi:10.1007/s00894-013-1928-3
13. N. Salimraftar, S. Noee, M. Abdouss et al., Three-level response surface full-factorial design: advanced chemometric approach for optimizing diclofenac sodium-imprinted polymer[J]. Polym. Bull. **71**, 19–30 (2014). doi:10.1007/s00289-013-1042-9
14. I.A. Nicholls, H.S. Andersson, K. Golker et al., Rational design of biomimetic molecularly imprinted materials: theoretical and computational strategies for guiding nanoscale structured polymer development[J]. Anal. Bioanal. Chem. **400**, 1771–1786 (2011). doi:10.1007/s00216-011-4935-1
15. W. Dong, M. Yan, M. Zhang et al., A computational and experimental investigation of the interaction between the template molecule and the functional monomer used in the molecularly imprinted polymer[J]. Anal. Chim. Acta **542**, 186–192 (2005). doi:10.1016/j.aca.2005.03.032
16. X.L. Li, J. Luo, Y.W. Lin et al., Density functional theory investigation of nonsymmetrically substituted uranyl–salophen complexes[J]. J. Radioanal. Nucl. Chem. **307**, 407–417 (2016). doi:10.1007/s10967-015-4326-8
17. F.F. He, H.Q. Wang, Y.Y. Wang et al., Magnetic Th(IV)-ion imprinted polymers with salophen schiff base for separation and recognition of Th(IV)[J]. J. Radioanal. Nucl. Chem. **295**, 167–177 (2013). doi:10.1007/s10967-012-1891-y
18. N. Karthikeyan, J.J. Prince, S. Ramalingam et al., Electronic [UV-Visible] and vibrational [FT-IR, FT-Raman] investigation and NMR-mass spectroscopic analysis of terephthalic acid using quantum Gaussian calculations[J]. Spectrochim. Acta Part A **139**, 229–242 (2015). doi:10.1016/j.saa.2014.11.112
19. M. Dolg, H. Stoll, A. Savin et al., Energy-adjusted pseudopotentials for the rare earth elements[J]. Theor. Chim. Acta **75**, 173–194 (1989). doi:10.1007/BF00528565

20. A. Elkechai, Y. Mani, A. Boucekkine et al., Density functional theory investigation of the redox properties of tricyclopentadienyl- and phospholyluranium(IV) chloride complexes[J]. Inorg. Chem. **51**, 6943–6952 (2012). doi:10.1021/ic300811m
21. F. Dulong, J. Pouessel, P. Thuery et al., Nitrite complexes of uranium and thorium[J]. Chem. Commun. **49**, 2412–2414 (2013). doi:10.1039/c3cc39163a
22. C. Lee, W. Yang, R.G. Parr, Development of the Colle-Salvetti correlation-energy formula into a functional of the electron density[J]. Phys. Rev. B **37**, 785–789 (1988). doi:10.1103/PhysRevB.37.785
23. M.P. Andersson, P. Uvdal, New scale factors for harmonic vibrational frequencies using the B3LYP density functional method with the triple-ζ basis set 6–311 + G(d, p)[J]. J. Phys. Chem. A **109**, 2937–2941 (2005). doi:10.1021/jp045733a
24. J. Luo, C.M. Nie, W.Q. Shi et al., Theoretical studies on the AnO2(n+) (An = U, Np; n = 1, 2) complexes with di-(2-ethylhexyl)phosphoric acid[J]. Dalt Trans. **44**, 3227–3236 (2014). doi:10.1039/c4dt03321c